EPJ manuscript No.
(will be inserted by the editor)

Improvement of the extraction method of faint signals in γ-activity measurements of meteorites

D. Gardiol[1], D. Barghini[1,2], P. Colombetti[2], C. Taricco[1,2], S. Mancuso[1], S. Rubinetti[1,2] and M. Di Martino[1]

[1] INAF - Osservatorio Astrofisico di Torino (OATo) - Via Osservatorio 20, 10025 Pino Torinese (Italy)
[2] Università degli Studi di Torino - Dipartimento di Fisica - Via Pietro Giuria, 1, 10125 Torino (Italy)

Received: date / Revised version: date

Abstract. At the underground laboratory of Monte dei Cappuccini (OATo-INAF) in Torino (Italy) we set up selective HPGe-NaI(Tl) spectrometers for measurements of cosmogenic radioisotopes in meteorites in order to study centennial-scale modulation of solar activity. ^{44}Ti is a suitable proxy for this timescale, but its detection is difficult due to the strong interference by naturally occurring ^{214}Bi. In order to optimize the extraction of the ^{44}Ti signal, we have developed software procedures specifically designed to improve selectivity of the Ge-NaI detectors coincidence.

PACS. 07.85.Fv, 29.40.-n Gamma-ray detectors – 29.30.Kv Nuclear physics – 07.85.Nc Gamma-ray – 96.30.Za Meteorites – 96.50.S- Cosmic rays – 29.85.-c Nuclear data analysis

1 Introduction

The interdependence between solar activity, solar magnetic field and Galactic Cosmic Ray (GCR) flux and their variability on different time scales is still subject of study and debate [1],[2],[3]. Since the solar activity affects terrestrial climate, it is important to reveal the heliospheric magnetic field variations, especially long-term changes and centennial periodicities. Several proxies of solar activity (*e.g.* cosmogenic radionuclides in terrestrial archives) suggest the presence of centennial and multi-centennial variations; however they are also influenced by terrestrial phenomena, such as geomagnetic field, climatic changes and deposition rate variations, all of which tend to mask the modulation due to solar activity. Cosmogenic isotopes produced in meteorites during their exposure to GCR in the interplanetary space can provide a direct measure of the GCR flux, avoiding terrestrial influences. We previously demonstrated that an ideal isotope for studying centennial-scale variability is the radioactive nuclide ^{44}Ti ($T_{1/2} = 59.2 \pm 0.6$ years) produced by spallation reactions, mainly due to cosmic ray protons in Fe and Ni in the body of a meteoroid. At the underground laboratory of Monte dei Cappuccini (Torino), the Cosmogeophysics group measured ^{44}Ti activity in 20 chondrites which fell during the period 1766 to 2001, with selective high-resolution gamma-ray spectrometers [4],[5],[6],[7],[8]. We have also shown that ^{44}Ti is useful to assess solar activity reconstructions obtained from different models [9],[10].
We describe here a recent development in the analysis routines to extract ^{44}Ti activity from the measured γ-spectra. In sect. 2 we describe the detector and the coincidence method, while in sect. 3 we illustrate the analysis software we developed and some application examples. We draw the conclusions in sect. 4.

2 Meteorites measurements at Laboratory of Monte dei Cappuccini (Torino)

In order to measure γ-activity of meteorites, we set-up HPGe-NaI(Tl) spectrometers at the underground (70 m.w.e depth) Laboratory of Monte dei Cappuccini (OATo-INAF) in Torino (Italy). The most performing system consists of a hyperpure Ge detector (3 kg, 147% relative efficiency) surrounded by a NaI scintillator (90 kg) and housed into a thick Pb-Cd-Cu passive shield. It has a resolution of 1.85 keV and a peak-to-Compton ratio of 104 for the 1332.5 keV ^{60}Co γ-rays. This compound spectrometer has been upgraded by a multiparametric data acquisition [11], [12] allowing also spectroscopic detection of the NaI signal. Therefore it is possile to obtain different coincidence spectra and perform a posteriori data reduction and analysis, as we will describe in detail in sec. 3.
^{44}Ti decays by electron capture in an excited state of ^{44}Sc, which emits disexcitation γ-photons, with energy of about 68 keV, 78 keV and 146 keV. ^{44}Sc mainly undergoes β^+ decay into ^{44}Ca with emission of a photon of about 1157 keV.

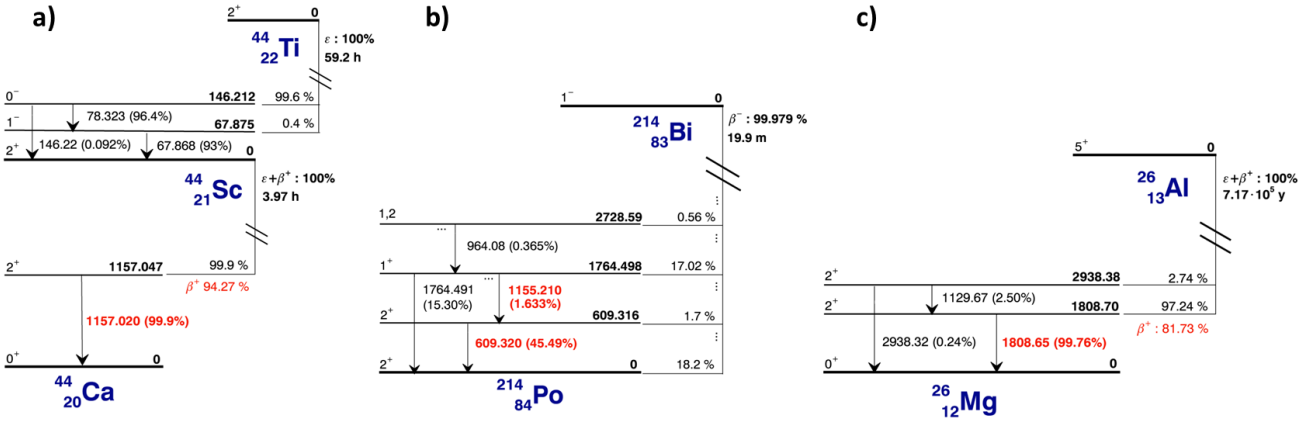

Fig. 1. Decay chains of a) ^{44}Ti; b) ^{214}Bi decay; c) ^{26}Al decay.

This decay is represented in fig. 1a. ^{44}Ti disexcitation photons are difficult to detect as they are at the lower limit range of an HPGe device, located in a region where the background level is high mainly due to electronic noise. Therefore, we reveal ^{44}Ti activity through the detection of the ^{44}Sc disexcitation photon at 1157 keV. However, this line is affected by the interference of a nearby line at about 1155 keV, that comes from β^- decay of naturally occurring ^{214}Bi nuclide of ^{238}U chain (see fig. 1b), at a distance in energy from ^{44}Sc line close to the resolution limit of the instrument. As described in [5], to overcome this problem we take advantage of the contemporary emission of two annihilation photons of the β^+ decay of ^{44}Sc which can be detected by NaI scintillators. However, ^{214}Bi has a high number of disexcitation γ-photons in the 511 keV and 1022 keV regions, in particular at about 609 keV. Because of the poor resolution of NaI scintillator, this can lead to false positives under the ^{44}Sc peak and, consequently, to peak interference. In general the 511 keV region is more sensible to this kind of cross-talk with respect to the 1022 keV region; on the other hand, the probability of detecting both annihilation photons (corresponding to 1022 keV coincidence) is lower with respect to the probability of detecting only one of this two photons (corresponding to 511 keV coincidence), resulting that 511 keV coincidence has a better statistic than 1022 keV coincidence. These two opposite effects are combined with differents weights, depending basically on the date of fall of the meteorite, and affect the two coincidence modes (see subsect. 3.5).
The key to achieve the best selectivity for ^{44}Sc with respect to ^{214}Bi events is to identify the appropriate energy range on NaI spectrum to efficiently extract ^{44}Ti events. In order to reveal the β^+ decays we explore the β^+ decay of ^{26}Al (a cosmogenic nuclide easily revealed in meteorites) into ^{26}Mg, mainly with emission of a about 1809 keV photon (see fig. 1c).

3 Description of Analysis Software

3.1 Software Features

The first step of the analysis software is the conversion of the data acquired by the Ge and NaI detectors into a 2D histogram with Ge channels in x-entries and NaI channels in y-entries. An example is given in fig. 2 (Dergaon meteorite, date of fall 2001 [13]; we will refer to data from this recently fallen meteorite to illustrate the features of our software (all routines are written in Interactive Data Language, IDL Exelis). This histogram contains all the information needed for the analysis. The total Ge spectrum is computed integrating over the full range of y-entries whereas integrating over a limited NaI range we obtain the so-called Ge *direct* coincidence spectrum. Similarly, integrating over the x-entries we obtain the NaI total and counter-coincidence spectra. The names *direct-* and *counter-* coincidence are assigned considering the HPGe device as the main detector and the scintillator as a secondary (guard) detector. Anti-coincidence spectra (*i.e.* spectra containing counts on one detector that are not in coincidence with any event on the other detector) are located in corrispondence of abscissa and ordinate axes. In order to avoid dependence from measurement time and meteorite sample mass, instead of integrated counts under a peak we will use their normalisation in time and mass unities (counts per minute per kilogram, cpm/kg). In the text, to simplify notation, we will use the symbol cpm for this quantity.
The second step in the analysis consists of the channel calibration of HPGe detector. An automatic search of photopeaks is performed over the total spectrum; then a 2^{nd} degree polynomial is used to fit the channel *vs.* keV and channel

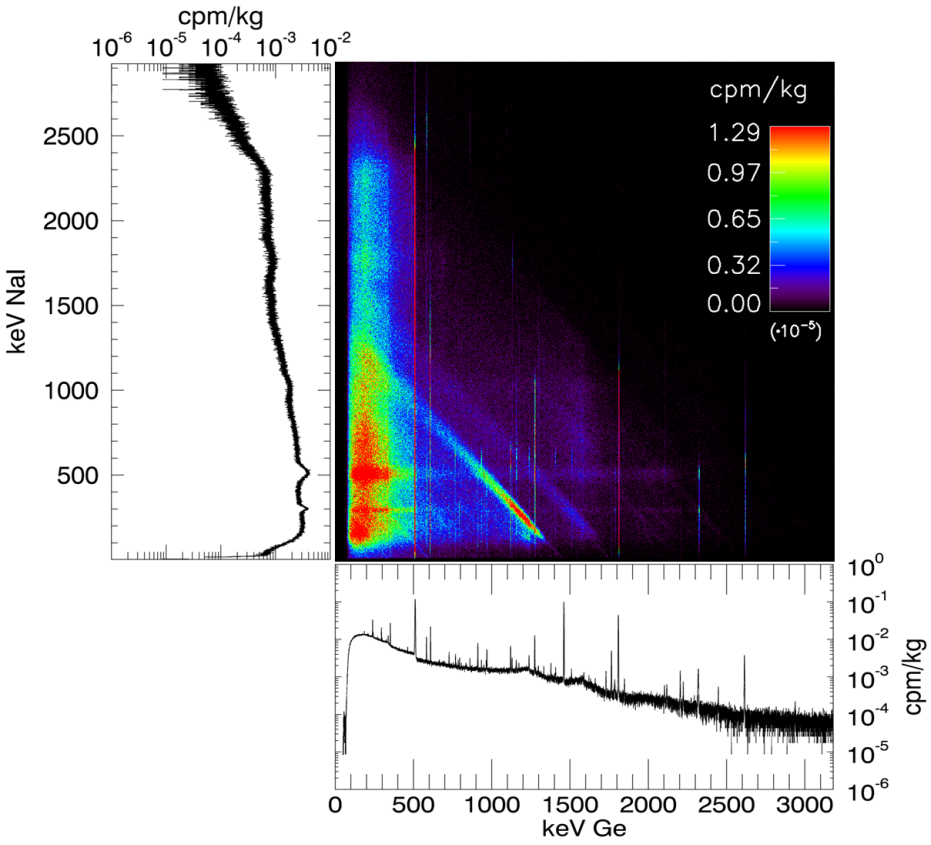

Fig. 2. Surface representation of the 2D Ge-NaI histogram of data from Dergaon meteorite, with total Ge and NaI spectra plotted on corresponding axes.

vs. FWHM profiles. Each spectral peak is fitted using a modified gaussian function with an underlying continuum together with asimmetrical terms [14]. In order to have fitting procedure converge in case of low statistic peaks, both peak position and FWHM parameters are fixed, calculated from calibration, thus resulting in variance reduction [11] [12]. The fitting procedure used to calibrate the NaI scintillator would lead to huge errors due to the large peak width; therefore we use information contained in the 2D histogram. Referring again to fig. 2, vertical lines represent counts of photons of a fixed energy on HPGe detector in coincidence with an energy spectrum on NaI scintillator; for instance, the vertical line at 1809 keV represents ^{26}Al photons detected on HPGe in coincidence with the annihilation spectrum and similarly for the horizontal lines. The different width of horizontal and vertical lines reflects the resolution of the two detectors. Furthermore, one can clearly see oblique lines: they can be interpreted as photons that passed through both detectors and deposited there two different fractions of their energy. The position of the left end of these sharper lines onto the NaI axis provide a more precise although indirect energy calibration.

3.2 Coincidence Routine

Fig. 3 (panels a,b,c) shows Ge total spectra of three meteorites (Dergaon, date of fall 2001; Dhajala, 1976 [15] and Agen, 1814 [8]) with different years of fall in the energy range of interest, corresponding to ^{44}Sc (green line) and ^{214}Bi (red line) peaks. In fig. 3a (Dergaon meteorite) we can clearly see that the ^{44}Sc peak dominates and the estimation of ^{44}Ti activity is easily given. In fig. 3b (Dhajala meteorite) the two peaks have comparable amplitudes and in fig. 3c (Agen meteorite) ^{44}Sc peak is barely seen. Fig. 3 (panels d, e, f) shows Ge coincidence spectra of the same meteorites resulting from the optimisation ruotine, using both 511 and 1022 keV NaI coincidence windows. This example shows that the coincidence is essential for old meteorites. In order to distinguish the signal we want to measure from the source of interference it is necessary to identify the energy spectrum of annihilation photons; fig. 4a shows two counter-coincidence spectra of Dergaon meteorite under ^{26}Al peak at 1808.65 keV (green) and ^{214}Bi peak at 1120.29 keV (red). In the ^{26}Al spectrum we can identify two peaks: the first (511 keV) corresponds to the detection of a single annihilation photon, whereas the second peak (1022 keV) corresponds to the detection of both annihilation photons. The continuum underlying this two peaks can be attributed to partial acquisitions of one or both photons. We will

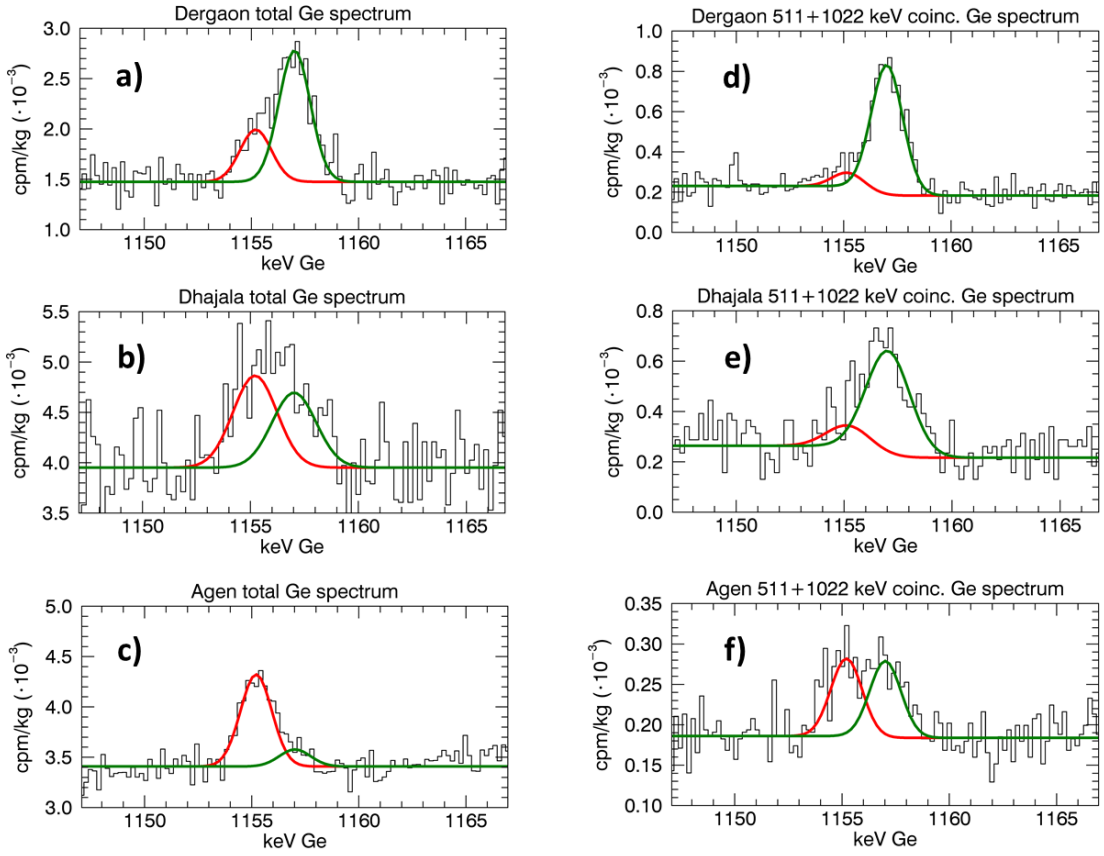

Fig. 3. Left side: Ge total spectra of different meteorites in the energy range of 1147-1167 keV: a) Dergaon meteorite (date of fall 2001); b) Dhajala meteorite (date of fall 1976); c) Agen meteorite (date of fall 1814). Right side: corresponding Ge coincidence spectra obtained using both 511 and 1022 keV windows. Superimposed lines represent the result of a Levemberg-Marquardt parametric fit for ^{214}Bi peak at 1155.020 keV (red) and ^{44}Sc peak at 1157.210 keV (green).

refer to coincidence ranges around these two peaks as 'windows' or 'coincidence windows'. The ^{214}Bi spectrum clearly shows the peak corrisponding to about 609 keV photons from ^{214}Bi and its relevant superposition with the 511 keV peak.

Taking advantage of the multiparametric data acquisition system, we can explore all possible coincidence windows and decide *a posteriori* which is the most performing one according to a quantitative criterium (figure of merit). To do that, we define the parametrization of the ensemble S of all possible coincidence windows through their centre c and the half-width w; then we extract coincidence spectra from the 2D histogram for each point of the ensemble and compute, over each spectrum, a parametrical Levemberg-Marquardt fit (implemented in IDL through the MPFIT procedure [16]) over ^{44}Sc - ^{214}Bi and ^{26}Al regions. The result of this procedure is a set of 2D matrices containing the values of all relevant fit parameters (*e.g.*: counts, FWHM, signal-to-noise ratio,...) as functions of (c, w). Regarding the sampling density in S in terms of (c, w), since the NaI scintillator has a linear energy calibration parameter of 0.183 ± 0.05 keV/channel, small compared to the peaks FWHM (30-40 keV), variations of few acquisition channels are not relevant; oversampling should be avoided and steps between 5 and 20 channels are appropriate and lead to a satisfying and still high sampling density. In fig. 5 we give the map representation of some of these matrices, referring to 511 keV window; we will focus on this coincidence mode as it is the most challenging and sensible to ^{214}Bi interference. The triangular shape of this figures is due to the requirement of fixed boundaries of the explored NaI range.

3.3 Figure of merit

The ^{44}Sc and ^{214}Bi cpm maps (Fig. 5 show a maximum associated to the biggest coincidence window and the trivial increasing trend of counts to as the window gets wider; this two maxima are superimposed, so that great values of

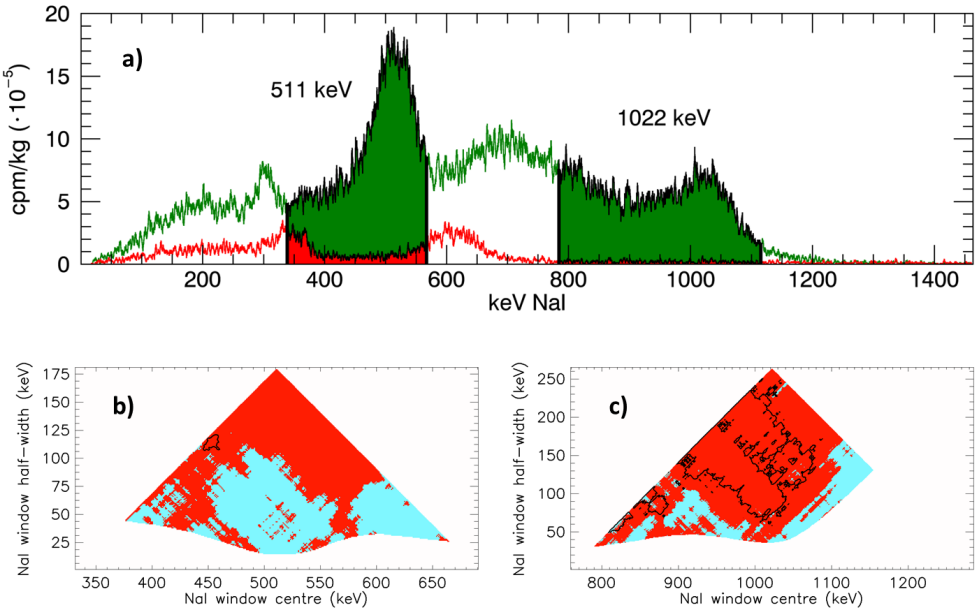

Fig. 4. Results for coincidence windows optimisation for Dergaon meteorite: a) represents the two coincidence windows chosen by the optimasation procedure, superimposed on the two NaI counter-coincidence spectra of ^{26}Al line at 1808.65 keV (green) and ^{214}Bi line at 1120.29 keV (red); b) and c) reprentents G region boundary (solid black line), F region (red) and $S-F$ (blue) respectively for 511 and 1022 keV, with a cut-off for very small windows imposing $\tilde{R}_{Al} \geq 0.05$.

^{44}Sc cpm correspond to similar high values of ^{214}Bi cpm, within the variability range. Similar tendency can be noticed in signal to noise ratio (SNR) map, even if the point of maximum is not strictly confined to the widest window; in our case, SNR is defined as:

$$SNR = \frac{cpm}{\sigma_{cpm}}, \tag{1}$$

where σ_{cpm} is given by the fit procedure. Recalling sect. 2, our aim is to minimise the cross-talk and maximise the usually scarce SNR due to low statistics of ^{44}Ti events. By applying a normalisation to remap the cpm range variability between 0 and 1, a possible figure of merit can be defined as:

$$M = cpm^*_{Sc} \cdot (1 - cpm^*_{Bi}) \cdot SNR^*_{Sc} \qquad cpm^*_{Bi} \in [0,1] \quad cpm^*_{Sc} \in [0,1], \tag{2}$$

where the *(c,w)* dependence is omitted and the asteriscs mean that quantities are evaluated in coincidence mode. Remapping cpm variability range into a standard interval is also useful to compare measurements of different meteorites. According to this definition, the choice of the coincidence window is performed by maximising the figure of merit:

$$(c_0, w_0) = \underset{(c,w)\in S}{argmax}[M(c,w)]. \tag{3}$$

Fig. 6a shows the map representation of the figure of merit in the case of 511 keV region. We can notice that M is a smooth function of *(c,w)* and, in particular, the coincidence window that maximes M is not a singular spot but it is located in a region of similar high values; this check is a fundamental step to confirm the result of the maximisation condition, as we expect that values of cpm and SNR do not vary radically for small variations of window's centre and width with respect to the FWHM in this region. Therefore, in order to identify a proper maximum (c_0, w_0) we have to require that at least in a neighbourhood of (c_0, w_0), $M(c,w)$ is smooth. This consideration also explains the particular choice of the expression of M, which avoid the simply maximising cpm_{Ti}/cpm_{Bi} fraction potentially leading to singularities of M for small values of cpm_{Bi}.

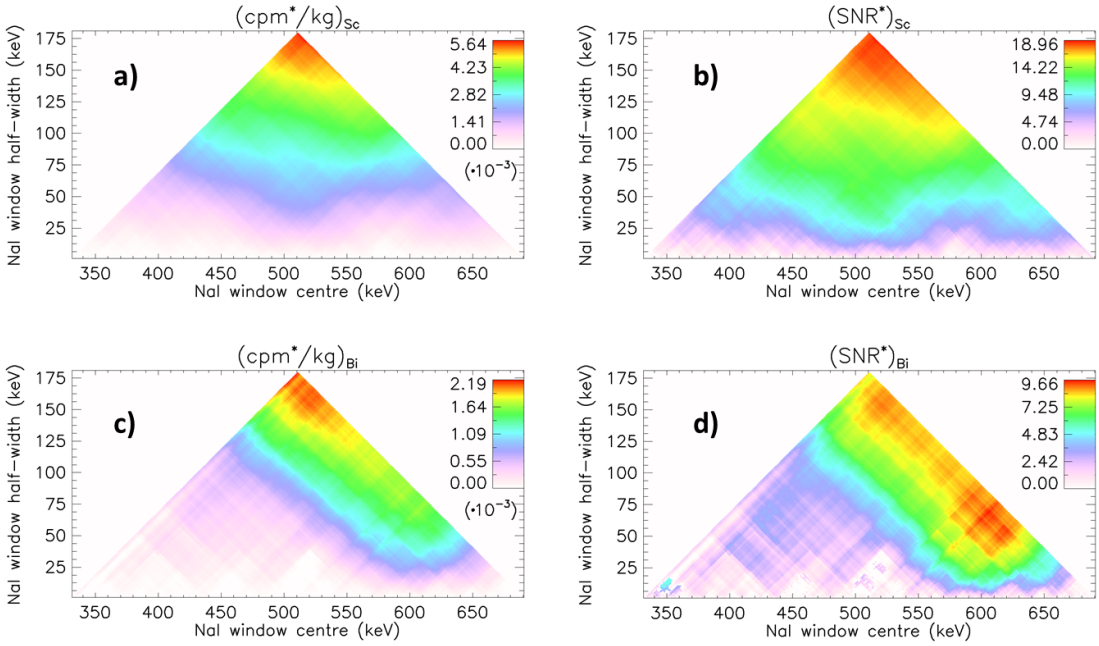

Fig. 5. Map representation of relevant quantities computed by coincidence routine in the case of 511 keV range for Dergaon meteorite measurement.

3.4 Normalisation of coincidence counts

As described in sect. 2, we exploit the β^+ decay of ^{26}Al to compute a normalisation factor useful to deduce ^{44}Ti activity. We can therefore define the estimator of coincidence to total counts ratio R for a generic coincidence line as:

$$\tilde{R}(c,w) = \frac{cpm^*(c,w)}{cpm}, \tag{4}$$

where *cpm* is the total Ge spectrum counts in time and mass unities of the selected line and the tilde designates that this is an estimator. Fig. 6b shows the map representation of $\tilde{R}_{Al}$ computed by our software in the 511 keV region. Under the hypothesis that ^{26}Al and ^{44}Sc β^+ decays happen with a similar dynamic, we can make the assumption that:

$$R_{Al} = R_{Sc}, \tag{5}$$

and therefore estimate ^{44}Sc total cpm as:

$$cpm_{Sc}(c,w) = \frac{cpm^*_{Sc}(c,w)}{\tilde{R}_{Al}(c,w)}. \tag{6}$$

This assumption is essential because we are obviously unable to directly estimate R_{Sc}. On the other hand, since the ^{26}Al and ^{44}Sc information is extracted from the same data sample, $\tilde{R}_{Al}$ already cointains the evaluation of effects such as self-absorption of the meteorite and NaI scintillator efficiency. The estimation of ^{44}Sc total cpm given by (6) depends on the window parametres (c,w) while the expected value must be unique. Theoretically this would imply ^{44}Sc total cpm map to be flat. However cross-talk affecting the numerator or discrepancy between R_{Al} and R_{Sc} affecting the denominator can introduce a spread in cpm values; in practice, we require to have a flat behaviour of normalised cpm map at least in a limited region $G \subseteq S$ around the chosen coincidence window (c_0, w_0). The exact definition of G is somewhat arbitrary. Taking into account sect. 3.3, and defining:

$$M_0 \equiv M(c_0,w_0) \quad \text{and} \quad cpm_0 \equiv cpm(c_0,w_0), \tag{7}$$

for our purpose G can be identified using a 1-σ confidence interval and expressed as:

$$G = \{(c,w) \in S : |M_0 - M(c,w)| \leq \sigma_{M_0}\}. \tag{8}$$

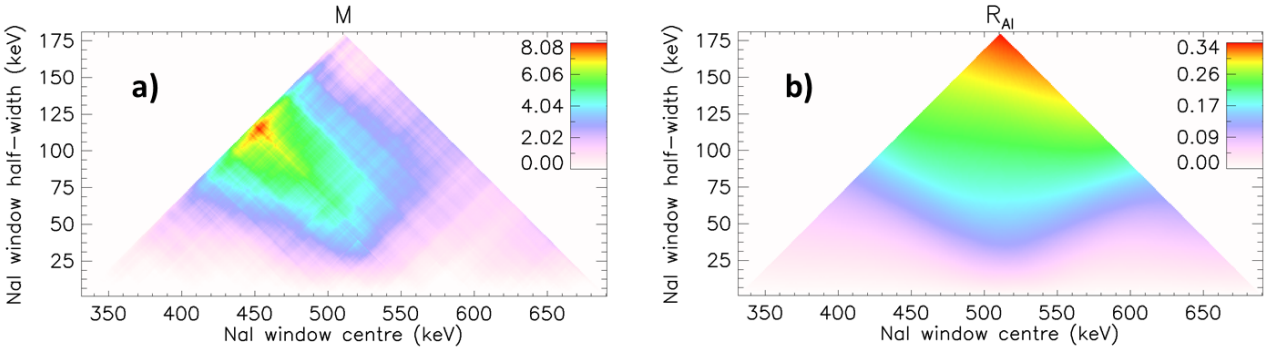

Fig. 6. Map representation for 511 keV Dergaon coincidence of: a) figure of merit M; b) coincidence *vs.* total counts ratio estimator $\tilde{R}$ for ^{26}Al peak at 1808.65 keV.

Similarly we can define the cpm_{sc} compatibility region F as:

$$F = \{(c, w) \in S : |cpm(c, w) - cpm_0| \leq \sigma_{cpm_0}\}. \tag{9}$$

Therefore the flatness requirement translates into:

$$G \subseteq F. \tag{10}$$

Fig. 4b and 4c shows the regions F and G for the 511 and 1022 keV region respectively. In both cases the flatness requirement is substantially satisfied. In the first case the algorithm chooses a well-defined coincidence window which position is shifted to the left with respect to 511 keV peak maximum, reflecting the already cited presence of 609 keV interference peak from ^{214}Bi decay. In the second case, the G region is much more extended. Possible reasons are: a) the lower statistic of double with respect to single detection of annihilation photons; b) the absence of significant interference lines in this regions. Fig. 4a shows the chosen coincidence windows superimposed to the two NaI counter-coincidence spectra.

3.5 Further examples and results

As a final step, we show the application of this optimisation method on data from Dhajala and Agen meteorites measurements (see sect. 3.2), for which we provide in fig. 7 the representations of F and G regions in both 511 and 1022 keV coincidences.

Dergaon, Dhajala and Agen G regions have similar features and the flatness requirement is satisfied also in the two latter cases. In the specific case of Agen 511 keV region (fig. 7c), the absolute maximum of M corresponds to a NaI window that introduces spurious ^{44}Sc counts and this effect is not already taken into account by our definition of the figure of merit. Nevertheless, M presents a sharp local maximum (shown in the figure) corresponding to the G region suitable for our purpose. Table 1 summarises values of M, cpm_{Sc}, SNR and optimised parameters (c, w) for the coincidence windows selected. In the same table we list also the results for Ge spectra containing events from both 511 and 1022 keV optimised coincidence windows. It can be noticed that, in all cases, the cpm_{Sc} values for the different coincidence modes are compatible.

	511 keV				1022 keV				511 + 1022 keV	
Meteorite	M	$(c, w)^{[a]}$	$cpm_{Sc}{}^{[b]}$	SNR	M	$(c, w)^{[a]}$	$cpm_{Sc}{}^{[b]}$	SNR	$cpm_{Sc}{}^{[b]}$	SNR
Dergaon	8.1 ± 1.0	(453,114)	15 ± 1	15	8.2 ± 5.0	(950,165)	14 ± 1	14	13.9 ± 0.7	20
Dhajala	5.8 ± 0.9	(455,90)	17 ± 2	8	4.7 ± 2.4	(1028,179)	13 ± 2	6	13 ± 2	8
Agen	1.8 ± 0.3	(495,74)	2.7 ± 0.5	6	3 ± 1	(983,130)	2.4 ± 0.4	6	2.5 ± 0.3	8

[*a*] keV
[*b*] 10^{-3} counts/minutes/kg

Table 1. Results summary from the optimisation routines

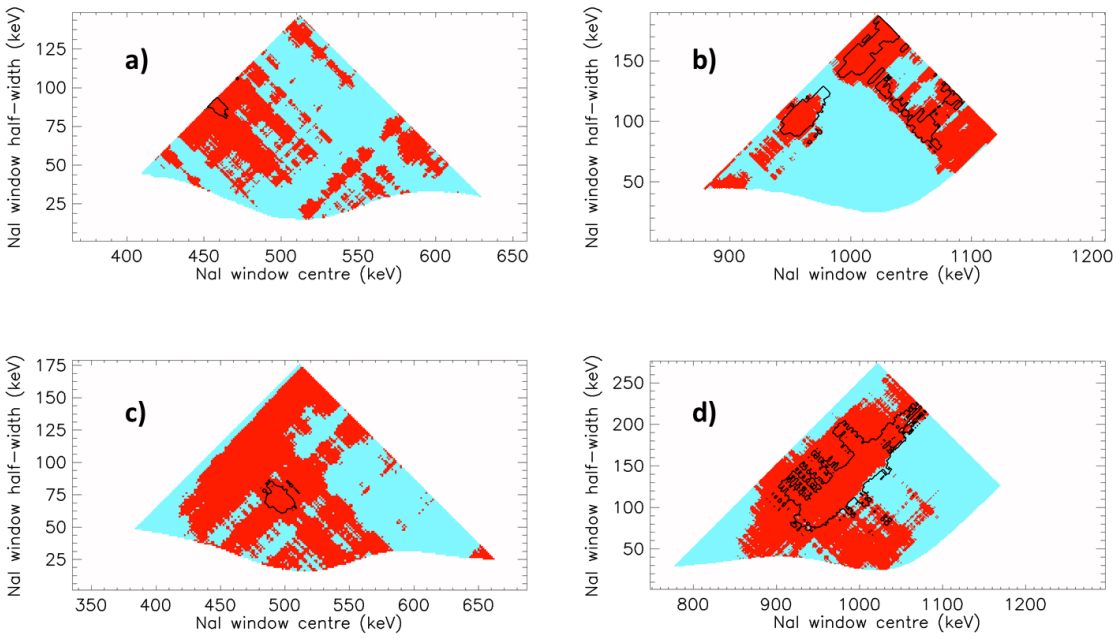

Fig. 7. F and G regions representation, as in fig. 4. Dhajala meteorite: a) 511 keV coincidence; b) 1022 keV coincidence. Agen meteorite: c) 511 keV coincidence; d) 1022 keV coincidence

.

3.6 Graphical User Interface

To manage this kind of data and easily visualise the map representation of matrices previously described, we developed a Graphical User Interface (see fig. 8). This GUI allows us to upload a specific dataset of a meteorite and provide an interactive view of ^{26}Al and $^{44}Sc - ^{214}Bi$ results for 511 and 1022 keV; the main plot is located on the top-left side of the widget, whereas a set of customisation tools are available in the bottom-left panel. For instance, cut-off values in the color table can be modified using the two scroll bars. The map can also be zoomed in the right side of the widget, to highlight details of the represented matrix. Selecting a particulare point $(c, w) \in S$ on this plots, the program computes all the results of that particular coincidence window and shows the coincidence spectrum.

4 Conclusions

The particular data reduction method we described for meteorite gamma activity measurements with an HPGe-NaI(Tl) spectrometer allows us to perform the time-coincidence analysis in order to reject interference events that affect ^{44}Sc line detection and to recover ^{44}Ti signal. One relevant feature of the software is the optimisation of the coincidence windows parameters using a custom defined figure of merit to be maximised. Application of this routine to selected datasets belonging to meteorites of different date of fall shows that, at least in the case of 511 keV coincidence region, maximum of the figure of merit is well-defined in the parameters space, while for 1022 keV coincidence region the choice of the window is still confined although in a larger parameters range, proving that the most important interference line at 609 keV is effectively rejected. The results of all coincidence modes are compatible. We plan to apply this method to the meteorite measurements that will be performed. The code can be easily adapted to analyse any other spectral lines related with events in time coincidence on the two detectors. At the same time, the software development is still ongoing in order to include in the GUI other data analysis routines.

References

1. Cane et al., Geophysical Research Letters **26**, (1999) 565-568.
2. Belov et al., Space Science Reviews **93**, (2000) 79-105.

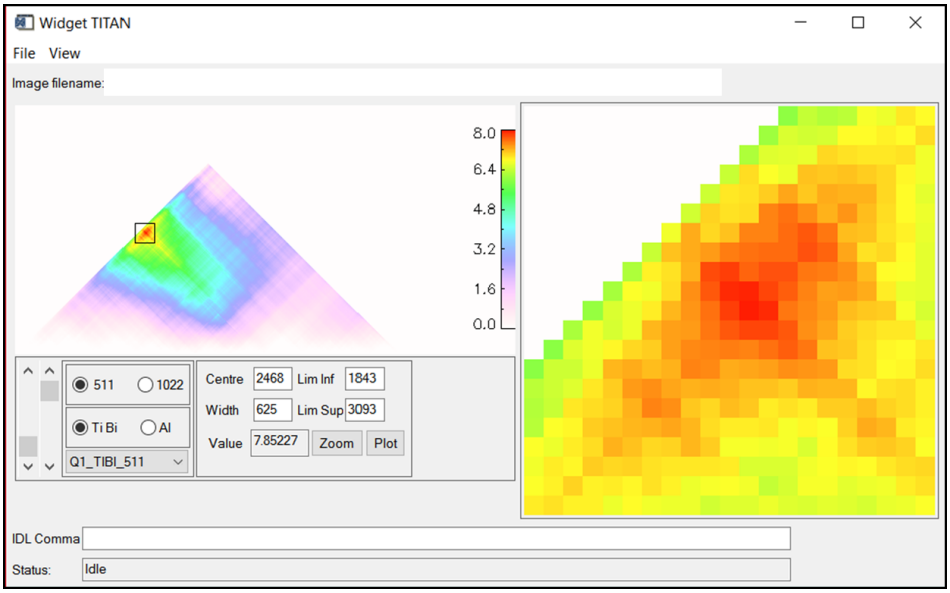

Fig. 8. Graphical User Interface (GUI) developed in IDL (Interactive Data Language) with the widget tool.

3. Rouillard and Lockwood, Annales Geophysicae **22**, (2004) 4381-4395.
4. Bonino et al, Science **270**, (1995) 1648-1650.
5. Taricco et al., Journ. of Geophys. Res **111**, (2006) A08102.
6. Taricco et al., Adv. in Space Res **41**, (2008) 275-279.
7. Taricco et al., Met. and Plan. Sci. **45**, (2010) 1743-1750.
8. Taricco et al., Astrophys. Space Sci. **361**, (2016) 338-342.
9. Usoskin et al., A&A **457**, (2006) L25-L28
10. Asvestari et al., MNRAS **467**, (2017) 1608-1613.
11. Colombetti et al., IEEE Nuclear Science Symposium Conference Record (2008) 18021805.
12. Colombetti et al., Nucl. Instr. and Methods in Phys. Res **718**, (2013) 140-142.
13. Taricco et al., Mem. S.A.It S. **14**, (2010) 177-179.
14. Simonits et al., JRNC **257**, (2003) 589595.
15. Taricco et al., Mem. S.A.It S. **80**, (2009) 284-286
16. Markwardt, Proceedings of the ADASS XVII conference, Québec City (2-5 november 2009), edited by David A. Bohlender, Daniel Durand, and Patrick Dowler, Vol. **411**, (2009)